Appendix D

Annual Report

A Surface Science Investigation of Fischer–Tropsch Catalysts

Principal investigator: Professor G.A. Somorjai

Researchers: E.L. Garfunkel, M.A. Logan, and Dr. J.J. Maj

OVERVIEW

The purpose of this project is to investigate various fundamental aspects of Fischer-Tropsch catalysts, using modern ultrahigh vacuum techniques in combination with classical reaction dynamic studies. The information obtained is used to help understand and develop catalysts that give a high specificity for useful products, such as olefins, oxygenates, and high molecular weight hydrocarbons. In this report, we concentrate on four areas of our research which have yielded the most interesting results. First, the results for CO hydrogenation reactions on rhodium foils and various rhodium oxides are discussed. For rhodium foils we find an inverse deuterium effect and develop a kinetic model consistent with the data. On various rhodium compounds we correlate the oxidation state of rhodium at the active sites with the observed product distribution. For example, $FeRhO_3$ produced a significant fraction of alkenes, while $LaRhO_3$ produced large amounts of oxygenated products. Second, we discuss our results for CO hydrogenation on promoted thorium compounds. These catalysts have proven to produce methanol at high rates and selectivities. Third, we describe our results on the effect of potassium promoters on small molecular adsorbates on platinum. Significant and informative changes in the chemisorption of CO and benzene are noted when coadsorbed with potassium. In the final section, we briefly review our results for CO hydrogenation on model Re, Fe, Pt, and Pd catalysts. Re and Fe both produce hydrocarbons at high rates, with Fe showing a better selectivity towards higher molecular weight products. Alkali metals enhanced the selectivity towards higher molecular weight products (and from alkenes to alkanes). Pt and Pd showed very low rates in comparison to Fe and Re but Pd proved interesting in that it yielded mostly methanol.

Experimental

Our studies have been carried out in three ultrahigh vacuum stainless steel chambers (see figure 1), pumped by ion and oil diffusion pumps, and achieve a base pressure of 10^{-10} torr.) The chambers are equipped with various ultrahigh vacuum features to clean and examine the surface of a given sample. These include a mass spectrometer for thermal desorption spectroscopy (see figure 2), low energy electron diffraction (LEED) for surface structure, Auger electron spectroscopy (AES,-See figure 3) to determine the atomic composition of the surface, and X-ray photoelectron spectroscopy (XPS, see figure 4) giving information on the oxidation state of major components on the surface, as well as some compositional information. An argon ion gun is used to clean the surface of the model catalysis samples. Molecular dosers connected to leak valves are used to expose the sample with known amounts of gases. Two of these chambers are also equipped with a high pressure cell, (see figure 1b), which is mounted on a piston driven bellows system. This cell can be closed over the sample, with 2000 psi sealing pressure, creating a loop to which high pressure (<20 atm) hydrogen and carbon monoxide mixtures can be added and circulated. In this way the system can be run as a batch reactor, with products detected by injecting samples into a gas chromatograph.

In some of the experiments, potassium was deposited using a "Saes Getters" source mounted 3 cm from the crystal. Deposition rates were typically 1 monolayer/ minute. Sulfur was deposited from an electrochemical source in vacuum.

Results

1.1 Rh foil

Studies on rhodium foil have found several unique features for the hydrogenation of carbon monoxide. A proposed reaction mechanism is shown in figure 5. For rhodium foil four assumptions can be made to help determine a model rate law for the formation of methane. First, the surface is nearly saturated with adsorbed carbon monoxide, as is seen by in situ infrared studies (Kellner & Bell). Second, all surface oxygen is removed as water, which is what we see using mass spectroscopy on this system. Third, all the steps in the mechanism indicated as being reversible are in fact at equilibrium. Fourth, the rate determining step is the formation of methane. Then for the case of rhodium foil where methane production is predominant, -96 mole percent, the model rate law for the reaction is given by $R_{CH4} = K \cdot P_{CO}^{-1} P_{H_2}^{+1.5}$. This form of rate law is expected for a competitive adsorption dissociation process.

If we now conduct experiments to find the rate law for methanation over rhodium foil by varying the partial pressure of the reactant gases, H_2 and CO, while holding the total pressure and temperature constant (see figure 6), we find the rate law, at 6atm total pressure and 300°C to be $R_{CH_4} = K P_{CO}^{-1} P_{H_2}^{+1}$. This corresponds well with our model and suggests that our proposed mechanism is fairly realistic.

An experiment performed to gain information about the rate determining step of the reaction is to substitute deuterium for hydrogen in the reactant gases. Two effects from this substitution can occur. First, the thermodynamic isotope effect, which is due to the difference in hydrogen and deuterium gas zero point energies and the respective

metal hydrogen or metal deuterium zero point energies. From the thermodynamic isotope effect more hydrogen should be present on the surface relative to deuterium. Second, the kinetic isotope effect, which is due to the activation energy difference between the $M-H \rightarrow C-H_x$ and $M-D \rightarrow C-D_x$ reactions, where $M-D \rightarrow C-D_x$ is the lower. The kinetic isotope effect predicts that deuterium will react faster than hydrogen with carbon on the surface. Experimentally we find (see figure 7) that the methanation reaction procedes faster with deuterium in the reaction mixture which would indicate that the rate determining step is in fact one of the hydrogenation steps of the reaction.

Some conclusions from the work on rhodium foil can be drawn at this point in our work. Rhodium foil is a stable syngas methanation catalyst with "mediocre" activity. It displays an inverse isotope effect which implies that one of the hydrogenation steps is rate limiting. The observed rate law for methanation follows our model rate law quite closely, indicating that the formation of methane from metal-CH_3 is probably rate limiting.

1.2 Rh Compounds

A number of Rh oxides were prepared and characterized following the procedure in Figure 8. The surface composition of each oxide, mounted on a gold foil, was determined by Auger electron spectroscopy. X-ray photoelectron spectroscopy was used to find the approximate oxidation state of the surface components. Thermal desorption measurements were carried out on Rh_2O_3, $LaRhO_3$, and Rh foil. The desorption temperature (top axis) and heat of desorption (bottom axis) for D_2 and CO thin film oxides are shown in figure 9. An anomalous CO desorption spectrum occurs for the used $LaRhO_3$ sample. Examination of the $LaRhO_3$ after running

the Fischer-Tropsch reaction shows two binding states for CO. One appears to correlate with the CO desorption from the fresh oxide. The appearance of the second peak may be a result of carbon deposited on the surface during the reaction, or may reflect a change in the oxidation state of the Rh at the catalyst surface.

There is an apparent correlation between the D_2 heat of desorption and the oxidation state of rhodium on the surface. The heat of desorption of the deuterium increases from 20 to 23 to 27 Kcal/mole as the oxidation state of the rhodium goes from 0 (Rh) to -1 (used Rh_2O_3, used $LaRhO_3$) to 3 ($LaRhO_3$, Rh_2O_3).

Product accumulation curves (figure 10) show a large change in the MeCHO/EtOH yields. This is due to a slow alteration in the nature of the catalyst surface during the reaction. After replenishment of the reactants, ethanol production resumes at essentially the same rate as at the end of the initial reaction while the ethanal production continues at a somewhat higher rate, but substantially less than its starting value. Additional evidence for catalyst aging is shown in the third section of figure 10). Here the sample has been treated by heating in oxygen (450 C 1×10^{-5} torr, 5 min) and cleaning by argon ion bombardment (1000eV, 5 μA for 30 min) before restarting the reaction. After this treatment the production MeOH and EtOH is very similar to the production rates under the initial conditions. Thus the gradual change in the product distribution is not linked to post reaction events, but is due to catalyst aging.

Rh_2O_3 has been shown to produce up to 25 wt. % of oxygenated products. This finding led the way to a possibility of selectively

producing higher energy products, alkenes, alcohols, and aldehydes, on rhodium compounds. Exploratory work has been done in several other rhodates (figure 11). From these initial results it appears that iron rhodate is a good candidate for further studies since the hydrogenation of carbon monoxide over it produces large quantities of alkenes. Lanthanum rhodate, $LaRhO_3$, produces up to 60 wt. % of oxygenated products. Copper rhodate, $CuRhO_3$, appears to have the same product distribution as rhodium foil but shows a much slower rate. When the sample is analyzed with AES and XPS after the reaction, it is found that rhodium has been reduced to rhodium metal and a partial copper overlayer has formed on the surface.

From work on the mixed rhodium oxides we have found several useful results. The rhodium in all the oxides tried partially reduces under the reaction conditions possibly creating more than one type of active site. By changing the structure and the other metal in the lattice we may be able to slow this tendency and thereby create a more product selective catalyst. The product distribution appears to be affected, to some degree, by three factors: structure of the oxide lattice, oxidation state of the active rhodium center and the other metal present in the lattice. Future work is planned to separate these effects.

2. Thorium Oxide

High surface area catalysts based on ThO_2 were prepared and evaluated for activity in synthesis gas reactions. Catalysts having surface areas on the order of 100 m^2/g were found to be highly selective towards the formation of alcohols, particularly methanol and isobutanol. These reactions, when carried out at moderate pressures (<100atm) and temperatures

(<350°C), showed ThO_2 catalysts to have higher activities and lower activation energies for methanol synthesis than the conventional ZnO based catalysts.

Surface analysis of active ThO_2 catalysts show them to have complicated structures, with substantial amounts of univalent impurity ions present. The role of the impurity ions in determining the defect structure of ThO_2 and the resulting effect on catalytic activity is currently under investigation.

3. Coadsorption Studies

An understanding of alkali coadsorption induced changes in transition metal catalysis is of great value in heterogeneous catalysis. In particular, potassium is used as a promoter on catalysts for the hydrogenation of carbon monoxide. In an attempt to understand the promoter effect, recent coadsorption experiments in our laboratory and others have shown that alkali metals change the chemisorptive characteristics of small reactive molecules (i.e. CO, H_2, N_2 and O_2) on catalyst surfaces. On iron and nickel surfaces, potassium appears to increase the heat of adsorption and the dissociation probability of CO. In addition, potassium increases the sticking probability of oxygen on platinum and bismuth and promotes oxide formation on iron, nickel, and bismuth surfaces. Also, both the heat of adsorption and the dissociation probability of N_2 increase on iron surfaces in the presence of potassium.

In the first study we have investigated the chemisorption of carbon monoxide on the platinum (111) surface in the presence of potassium as a model system. Due to the promoter action of potassium in Fischer-Tropsch reactions we believe that this type of ultrahigh vacuum/analysis on model catalyst surfaces is very important.

High resolution electron energy loss spectroscopy (HREELS) was used to determine the vibrational frequencies, thereby identifying the adsorption sites and relative site concentration of CO molecules when coadsorbed with potassium. Thermal desorption spectroscopy (TDS) provided information about changes in heats of adsortion of the coadsorbed system. Ultraviolet photoelectron spectroscopy (UPS) was utilized to determine the work function change of the surface as a function of potassium and CO coverage.

3.1 K + CO on Pt(111)

The preadsorption of potassium has marked effects on the adsorption of CO on Pt(111). Our main experimental findings can be summarized as follows:

i) The addition of submonolayer amounts of potassium continuously increases the heat of adsorption of CO on Pt(111) from 25 kcal/mole for clean Pt(111) to 36 kcal/mole for near monolayer coverages (see figure 12).

ii) Associated with the increase in heat of adsorption is a 310 cm^{-1} decrease in the stretching frequency of the bridge bonded CO molecules from 1870 cm^{-1} on clean Pt(111) to 1560 cm^{-1} with 0.6 monolayers of K coadsorbed (see figure 13).

iii) The CO thermal desorption peak broadens continuously to a maximum of 200K (full-width at half-maximum) at saturation CO coverages as the potassium coverage is increased.

iv) At a constant potassium coverage, the CO vibrational frequencies for both linear and bridge adsorption sites decrease substantially with decreasing CO coverage.

v) On the potassium-free Pt(111) surface, CO prefers to occupy top adsorption sites while on the potassium-covered surface CO adsorbs

preferentially on bridged sites.

vi) The work function of the Pt(111) surface decreases by 4-4.5 eV upon the adsorption of one-third of a monolayer of potassium, but increases by 1.5 eV when CO is coadsorbed (see figure 14).

These results can be interpreted by examining the electron acceptor character of CO and the changes in charge density at the platinum surface as potassium is adsorbed.

The bonding of carbon monoxide to metal atoms involves a synergistic electron transfer from the highest occupied molecular orbitals of CO (5σ) to the metal, and in turn metal electrons are backdonated into the lowest unoccupied molecular orbital ($2\pi^*$) of CO. The backdonation of metal electrons into the $2\pi^*$ orbital leads to a simultaneous strengthening of the M-C bond and a weakening of the CO bond, as seen in figure 15a, where the $d_{Pt} - 2\pi^*$ orbitals are in phase (bonding) between Pt and C, while being out of phase (antibonding) between C and O.

In our experiment changes in backdonation to CO are induced by using an electron donor, potassium (figure 15b). Charge is transferred from the potassium to the platinum, with electrostatic screening of the resultant positive charge on the potassium by metal electrons. This polarization is displayed by the 4-4.5eV drop in work function upon potassium adsorption (figure 14). Then, upon CO coadsorption, an enhancement (relative to clean Pt) of backdonation into the CO occurs as a result of the potassium induced surface charge density changes.

The 11 kcal/mole increase in adsorption energy of CO upon potassium coadsorption supports the model of enhanced electron backdonation.

In addition to strengthening the metal-carbon bond, backdonation should also weaken the carbon-oxygen bond as noted above, lowering its vibrational frequency. This indeed occurs since the vibrational frequency of bridge bonded CO at saturation coverage decreases by 310 cm^{-1} as the potassium coverage is increased to 0.6 monolayers.

The change in CO adsorption site from linear to bridged with increasing potassium coverage is a striking effect. Nieuwenhuys has recently shown that the degree of electron backdonation increases with the lowering of the work function of a metal surface. Our results not only indicate an increased heat of adsorption and decreased vibrational frequency due to the decreased work function, but also a change in CO site location. By continuously lowering the work function of the Pt surface by the adsorption of potassium, we are changing the most energetically favorable site location from top to bridged.

It must be noted that we cannot rule out the existence of the three-fold site CO molecule when the stretching frequencies decrease to their low coverage values. However, no clear evidence for the occupation of this site exists.

Although the Pt(111)/K system studied here is different from the multicomponent surfaces used on actual industrial catalysts, the catalytic implications of our results are significant, especially with respect to CO hydrogenation reactions. The increase in backdonation strengthens the M-C bond and weakens the C-O bond, thus increasing the ability of adsorbed hydrogen to react with CO. Furthermore, the increased binding energy means that the surface residence time of adsorbed CO will increase. It should also increase its probability of dissociation,

as is seen on iron and nickel. Both these consequences should lead to the formation of longer chain hydrocarbons, as is shown in our catalytic studies (see below).

In summary, the chemisorption properties of carbon monoxide are significantly altered when coadsorbed in the presence of potassium on Pt(111). The adsorption energy is increased by 11 kcal/mole and the CO vibrational frequencies decrease markedly. No dissociative adsorption was observed in our low pressure studies, although dissociation is induced by potassium on many other metals. These effects are explained by a simultaneous charge transfer from the potassium adatoms to the platinum substrate and an increase in backdonation from the platinum into the coadsorbed CO molecules. For a fixed potassium coverage, the CO molecules appear to compete for the "excess" charge donated by potassium. Direct bonding between coadsorbed CO and K is insignificant. Finally, a change in the CO site occupancy from top to bridge position is shown to occur with increasing potassium adsorption.

3.2 K + other small molecular adsorbates on Pt(111)

Following our extensive study of the interactions of CO with potassium (promoters), we examined the effects of potassium on other small adsorbed molecules in order to develop a general model of promoter action in cataysis. The interaction of co-adsorbed potassium with π-orbital containing molecular adsorbates (benzene, PF_3, NO, C_4H_8, and CH_3CN) on the Pt(111) crystal face was studied by thermal desorption spectroscopy. We found that co-adsorbed potassium significantly weakened the platinum-benzene bond. More of the benzene desorbed intact upon heating, instead of dissociating to yield H_2 and surface carbon.

Adsorbed NO was found to dissociate in an amount proportional to the K concentration, yielding N_2 and N_2O (as well as NO) in the desorption spectra. The adsorption of PF_3, C_4H_8 and CH_3CN was blocked by potassium, and no additional or shifted peaks were observed. We have developed a simple molecular orbital description to account for the potassium induced effects. The dominant idea is that only adsorbates having molecular orbitals with energy levels located near to E_f can be significantly affected by "electronic promotion" in catalysis.

3.2.1 Benzene

A fraction of the benzene adsorbed on clean Pt(111) will desorb intact upon heating, while the remainder dissociates giving off hydrogen. This behavior is also seen on other transition metals, such as Ni or Rh, but the Pt(111) surface appears unique in its low activity for C-C and C-H bondbreaking.

It has been proposed that dissociation of benzene occurs at steps or other defect sites because of geometric (steric) and/or electronic variations at these sites. We found that all of the adsorbed benzene dissociated upon heating for exposures of up to ≈ .7 L, and most of the additional benzene desorbed intact up to exposures of 2 L (see figure 16). For exposures greater than 2 L at room temperature the sticking coefficient became zero; presumably the first monolayer was saturated at this point. Thus, our results imply that benzene molecules on the flat Pt(111) surface can readily dissociate upon heating (as well as at step/defect sites) since the amount dissociated is much in excess of the estimated defect site concentration (<5%).

On Pt(111), that fraction of benzene that desorbs molecularly above room temperature yields two peaks in the thermal desorption spectrum at

approximately 375 and 450 K. The appearance of these two peaks is not yet fully understood although several interpretations are possible to explain their origin: lateral interactions at high coverages, different surface structures (as revealed by LEED), different sites being occupied (presumably top or threefold), etc.

Much more of the benzene desorbed intact upon heating when the Pt surface was pre-dosed with potassium: this is seen both from the larger thermal desorption peak area at low exposures (figure 17) as well as the smaller fraction of carbon that remains on the surface (as detected by AES) after heating. In addition, we observed a lower temperature for the benzene desorption rate maximum as potassium is added. Thus, desorption and decomposition should be viewed as competing reaction pathways: however, only the desorption energy (and pathway) is strongly affected by potassium coadsorption.

Both the decrease in desorption temperature and the increased amount of molecular desorption imply that the benzene-platinum bond strength is weakened when potassium is present. Several explanations can be proposed. Benzene is thought to be an electron donor in transition metal complexes, with the π-orbital often involved in a symmetric coordination with the metal atom or ion. Thus, one might expect that if the platinum surface is already "electron-rich" due to charge transfer from potassium, the benzene might not be able to donate charge, hence bond, as strongly.

This type of explanation however, is probably too simplistic, and a more complete understanding of the electron energy levels is required

to develop even a qualitative model of the potassium induced changes of adsorption. Figure 18 shows the molecular orbital diagram for benzene-chromium. Of interest here are the molecular orbitals involved near the "Fermi level," i.e. the highest occupied and lowest unoccupied molecular levels. All of the filled orbitals in the benzene chromium bond are either bonding or non-bonding between the benzene π-ring and chromium d-orbitals. The lowest unoccupied level, however, is "anti-bonding" between e_{1g} and chromium d-orbitals. Thus, if one electron were added to the system, this electron would fill the 2e level, weakening the metal-benzene interaction.

Of course there is quite a difference between a chromium atom and a platinum surface, but we believe that the general character of the bonding is the same: in both cases there is a symmetric coordination to the metal atom(s), and benzene can be considered primarily as an electron donor. For the platinum surface promoted with potassium, the Pt atoms can be considered to increase their electron density in the near surface region as they screen the slightly ionized potassium atoms. This surface polarization also drops the work function, and the platinum should then be able to donate charge more readily to adsorbates. If we assume similar bonding characteristics to the chromium complex, then the lowest unoccupied acceptor level of the benzene-platinum system is anti-bonding between the ring and the metal. Potassium should help populate this level, weakening the metal-ring bond. Another complementary effect would be the inability of benzene to donate charge into the metal if the population of the 6s Pt level was increased due to the potassium. We feel, however, that this is a minor perturbation in comparison to donation into the anti-bonding level, because the analogous

effect of bond weakening was not seen for CO. Recent calculations by A.B. Anderson et. al. show that changes in the occupation of the benzene e_{1g} antibonding level (2e in figure 18) cause changes in the bending of the hydrogen atoms on benzene toward or away from its surface.

3.2.2 Phosphorous trifluoride

Adsorbed phosphorous trifluoride was found to desorb intact from both clean and partially potassium covered surfaces at about 500K. The thermal desorption spectra also showed some peak broadening, and a slight decrease in desorption maximum temperature. The lack of a large effect was at first surprising, since we had expected to observe effects similar to those seen for the (K+CO)/Pt(111) system, i.e. a 200K increase in desorption temperature.

However, for PF_3 bound to a metal, the σ-donor energy level is located well below E_f at ≈ 8eV, while the 2π acceptor level is split into two levels, one located 4.5eV below E_f (see figure 19). Thus, the absence of significant potassium induced chemisorption changes in PF_3 could be explained by 1) assuming that the σ doner levels, and the bonding 2π-acceptor levels, are fully occupied prior to potassium coadsorption, and 2) that the nearest unoccupied PF_3 level is too far above E_f to be able to accept electrons from the metal, even upon potassium coadsorption. One explanation for the slight drop in PF_3 desorption temperature is that there could be a decrease in σ (PF_3) to s-band (Pt) overlap, resulting from a filling of the 6s Pt band when potassium is adsorbed as mentioned above.

For CO, which exhibits a large change in bonding when co-adsorbed with potassium, the 2π bonding orbital is located only ≈0.6-2.0 eV

below E_f. Here the potassium is able to enhance the d-2π overlap, which strengthens the M-C bond and weakens the C-O bond (since the 2π level is antibonding between the C and O atoms). CO is therefore more sensitive to changes in surface electron density.

3.2.3 Acetonitrile (CH_3CN)

CH_3CN desorbed mostly intact from Pt(111) as has been observed in previous studies. Some dissociation occurred upon heating, as was monitored by AES following the thermal desorption cycle. Preadsorbed potassium was found to effectively block sites for acetonitrile adsorption, as was observed for PF_3 and butene, but no shifts in desorption peak temperature or width were detected.

Acetonitrile is known to be σ-bonded to metals via the lone pair orbital of its nitrogen. No accessible back-bonding levels are located near E_f, so there is no possibility of additional charge transfer between the metal and the unoccupied molecular orbitals. Therefore no significant changes in bonding are expected and none were found upon co-adsorption of this molecule with potassium.

3.2.4 Butene

The stable structure of alkenes adsorbed on the Pt(111) surface at 300K is thought to be a $R-\overset{\diagup M}{C}-\underset{\diagdown M}{M}$ species. Thus one does not expect any accessible adsorbate energy levels to exist near E_f since the highest σ-bonded levels are usually 5-15 eV below E_f. The similar shape of the H_2 thermal desorption profiles following butene exposures with and without potassium pre-deposition is therefore to be expected, assuming that metal carbon bonding has an effect on the hydrogen desorption

temperature. The changes induced in the second H_2 desorption peak are difficult to interpret and will require more information on the nature of the CH_n fragments believed to be present at these temperatures. In any case, as alkylidynes are thought to be important intermediates in the Fischer-Tropsch reaction, it is interesting to note the absence of a large potassium induced effect here.

3.2.5 Nitric oxide

The general features of non-dissociative NO and CO adsorption on metals are similar. The major difference, for our purposes, is that the gas phase NO molecule has one electron in the $2\pi^*$ antibonding orbital, while CO has none. When NO was exposed to a potassium covered surface, it adsorbed dissociatively. The general feature observed with increasing potassium coverage is an increased yield of N_2 and N_2O in the desorption spectra. NO was found to react directly with K as observed for NO exposures on K multilayers; hence no K induced NO-Pt changes could be proven.

In summary, the bonding of benzene and CO to the platinum (111) surface is markedly altered upon the co-adsorption of potassium. The weakening of the benzene-metal bond and the strengthening of the CO-metal bond by co-adsorbed potassium can be explained by charge transfer into molecular orbitals of the adsorbates with energy levels near the Fermi level, E_f. The absence of significant bonding changes of adsorbed PF_3, CH_3CN, and C_4H_8 in the presence of potassium is analogously explained by the absence of accessible molecular orbitals for charge transfer within 2ev of $\approx E_f$.

4. CO hydrogenation on promoted (unsupported) Fe,Re,and Pt samples.

Following our ultrahigh vacuum studies (see above), we began a series of model CO hydrogenation experiments on well defined Fe, Re, Pd, and Pt catalysts. Using our high pressure/low pressure chambers, we were able to characterize a sample before and after reactions to check for surface impurity concentrations of K, O, S, N, C, etc. It was interesting to note that we were able to reproduce actual industrial (non-zeolytic) catalyst products, rates, and selectivities on our model catalyst foils and crystals. Recently we have been able to produce methanol with high selectivities on Pd foil. The runs usually were characterized by a brief induction time, followed by a long stable period which would slowly decay after several hours. As will be shown below, this decay is attributable to the slow build-up of a carbonaceous layer which poisoned the surface reactivity.

Methane was the dominant product on most samples studied, but higher molecular weight olefins and alkanes were also monitored. In figure 20 we show an example of an Arrhenius plot of various runs on rhenium foil. The results of the Arrhenius plots and the selectivities are displayed in figure 21. The turnover rates used are the maximum values reached by the catalyst following any induction period (usually <30 min. after initiation). The turnover frequency listed assumed an active surface number of sites of 10^{15} over which the catalyst was uniformly heated. This number is hard to know accurately for several reasons. We believe however, that it is correct within 50%, as our results are in good agreement with data from iron F-T catalyst at similar temperatures. In any case, it is the relative values, not so much the absolute ones, which are

needed to discuss promoter effects.

The main mechanism of F-T catalyst poisoning was carbon buildup. In figure 3 we show an iron foil Auger spectrum before a catalyst run. Figure 22 shows a close-up of the carbon peak after a reaction. The amount of carbon on the surface after a given run was a function of catalyst pretreatment, reaction temperature, and reaction time. Partial CO & H_2 pressures also are important in determining poisoning time as will be discussed below.

Several interesting features were found concerning this carbonaceous layer. The layer was either "graphitic" (unreactive) or "carbidic" (reactive) depending on the reaction conditions (as discussed by other authors). It also contained large amounts of adsorbed (or trapped) oxygen and hydrogen, as was noticed in the thermal desorption of adsorbed gases following the reaction. "Carbidic" carbon was the dominant species following low temperature, short reaction time runs. "Graphitic" carbon was the dominant species following high temperature runs, or after flashing any postreaction surface to >700K.

Another type of poisoning was found when sulfur was present on the surface. Sulfur could be put on the surface either by heating the iron or rhenium up to a high temperature (>1000K), where sulfur will become mobile enough to segregate to the surface upon cooling, or by chemical vapor deposition. Sulfur changed the selectivity (toward methane), and it poisoned the surface by decreasing the number of active sites. We are currently studying the distinctions between electronic and structural effects of sulfur poisoning. In figures 21 we show the selectivities for the Re and Fe surfaces following oxygen and alkali promotion. A

major problem occurred here concerning the number of active surface sites to be used in calculating turnover numbers. As noted by Goodman et. al, oxidation tends to increase the surface area of the catalyst, if the oxidation reaches only 10-20Å into the surface. A second, more complicating factor arises when one finds that the degree of oxidation is not only a function of catalyst pretreatment, but it is constantly changing throughout the reaction as a function of catalyst temperature and reaction time. Higher temperatures favor less oxygen incorporation in vacuum, but under a high CO pressure (>1 atm), this is perhaps compensated for by an increased rate of CO dissociation and subsequent oxygen incorporation. Thus, the values cited are the best values we could deduce from a knowledge of pre-and post-reaction surface content. AES and TDS (thermal desorption spectra) were used to help in this determination.

Platinum and palladium showed much lower reactivities than Fe and Re. Palladium did prove interesting in that we were able to produce methanol selectively. We believe that palladium's ability to hold large amounts of hydrogen in the bulk is related to its unique properties of hydrogenating CO directly. Others have shown that CO + H_2 go to methanol without dissociating the CO, but in their studies on supported catalysts, they claimed that Pd was in an oxidized state when it was doing the catalysis. We have now shown that the reaction runs on the reduced Pd as well.

HIGH PRESSURE / LOW PRESSURE CHAMBER FOR CATALYST SURFACE STUDIES

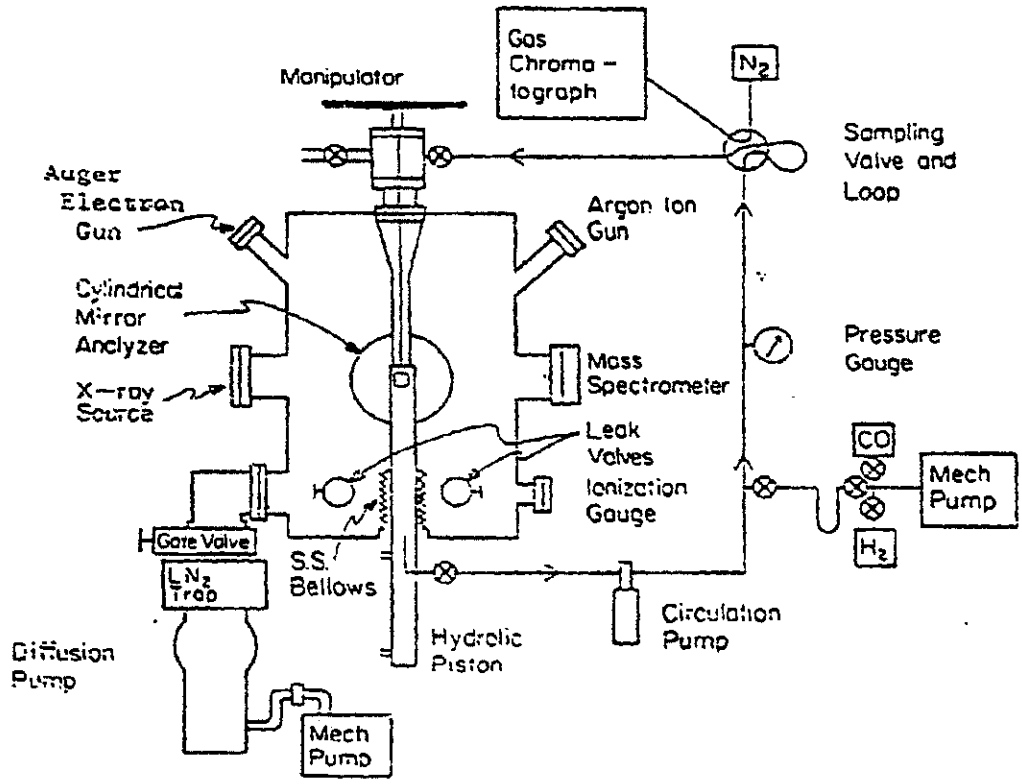

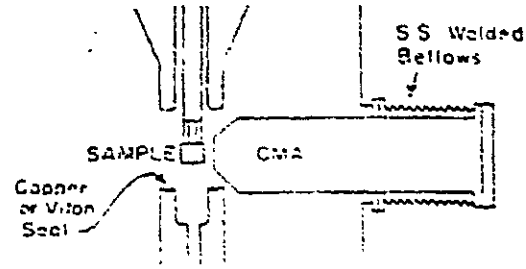

SIDE VIEW WITH HIGH PRESSURE CELL OPEN

Figure 1

Schematic representation of a chamber used to do both high pressure catalvsis and ultrahigh vacuum studies.

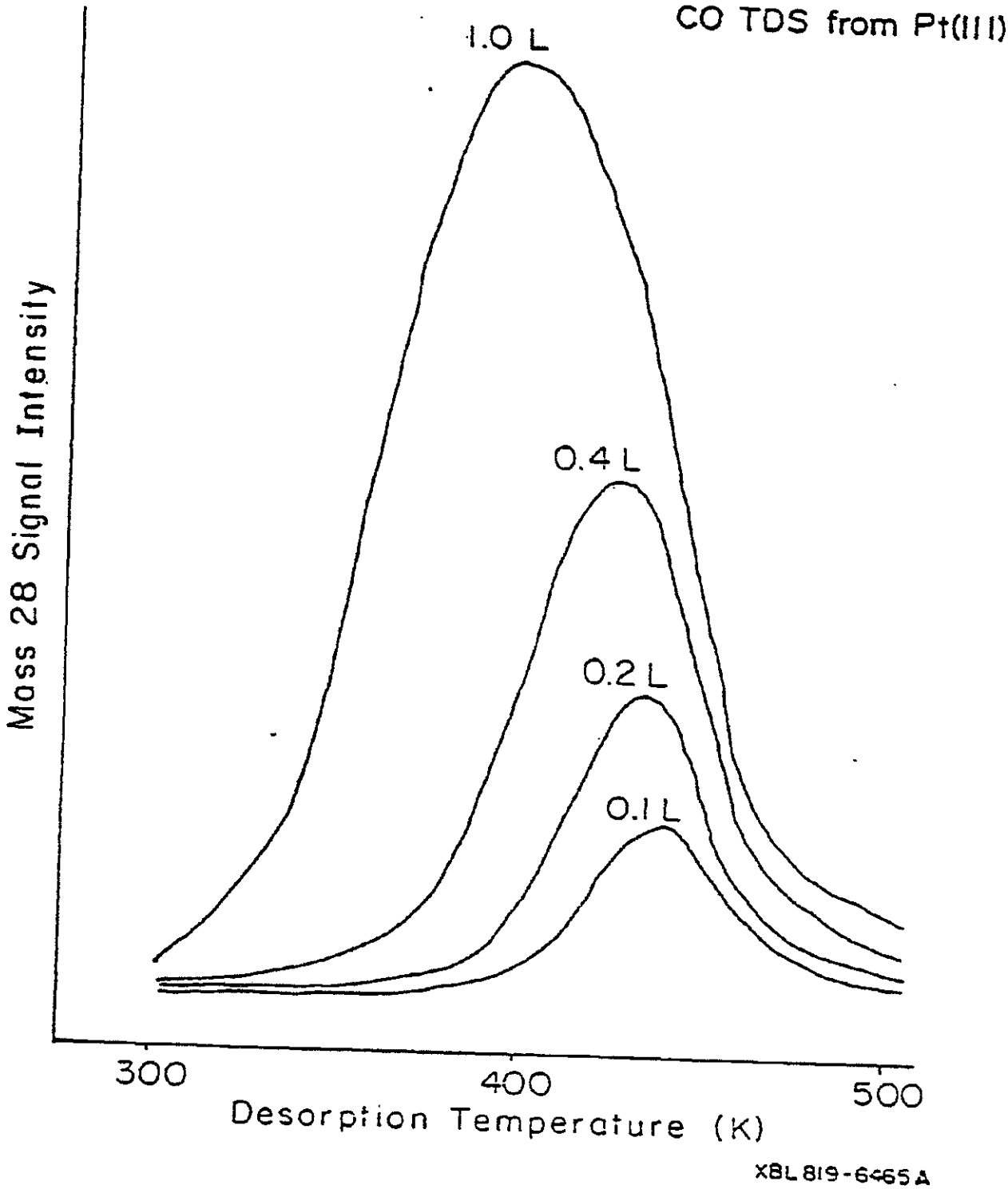

Figure 2

Thermal desorption spectra of CO from clean Pt(111) for various CO coverages (expressed in terms of Langmuirs).

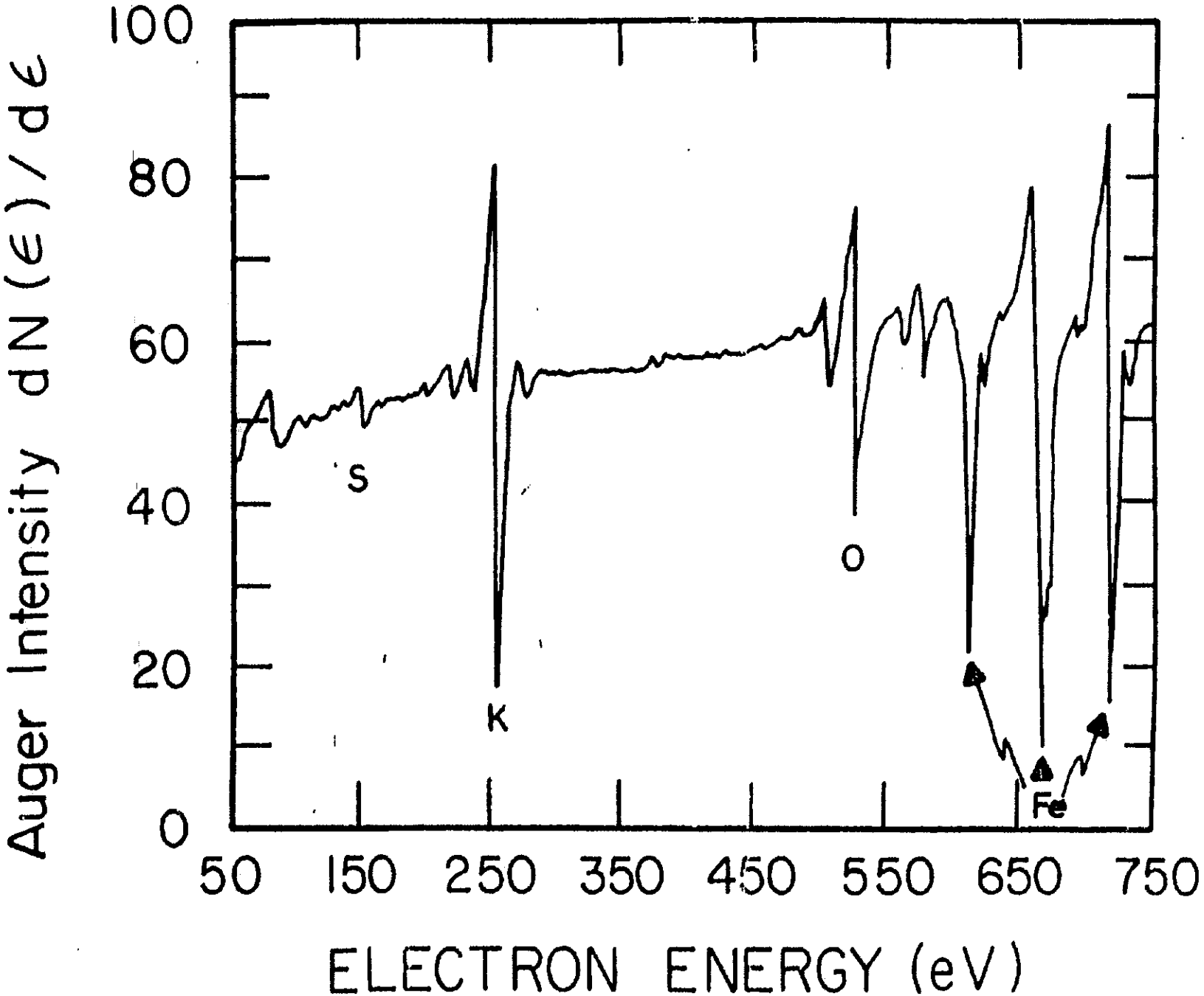

Figure 3

Auger derivative spectrum for potassium doped iron foil. Note oxygen impurity.

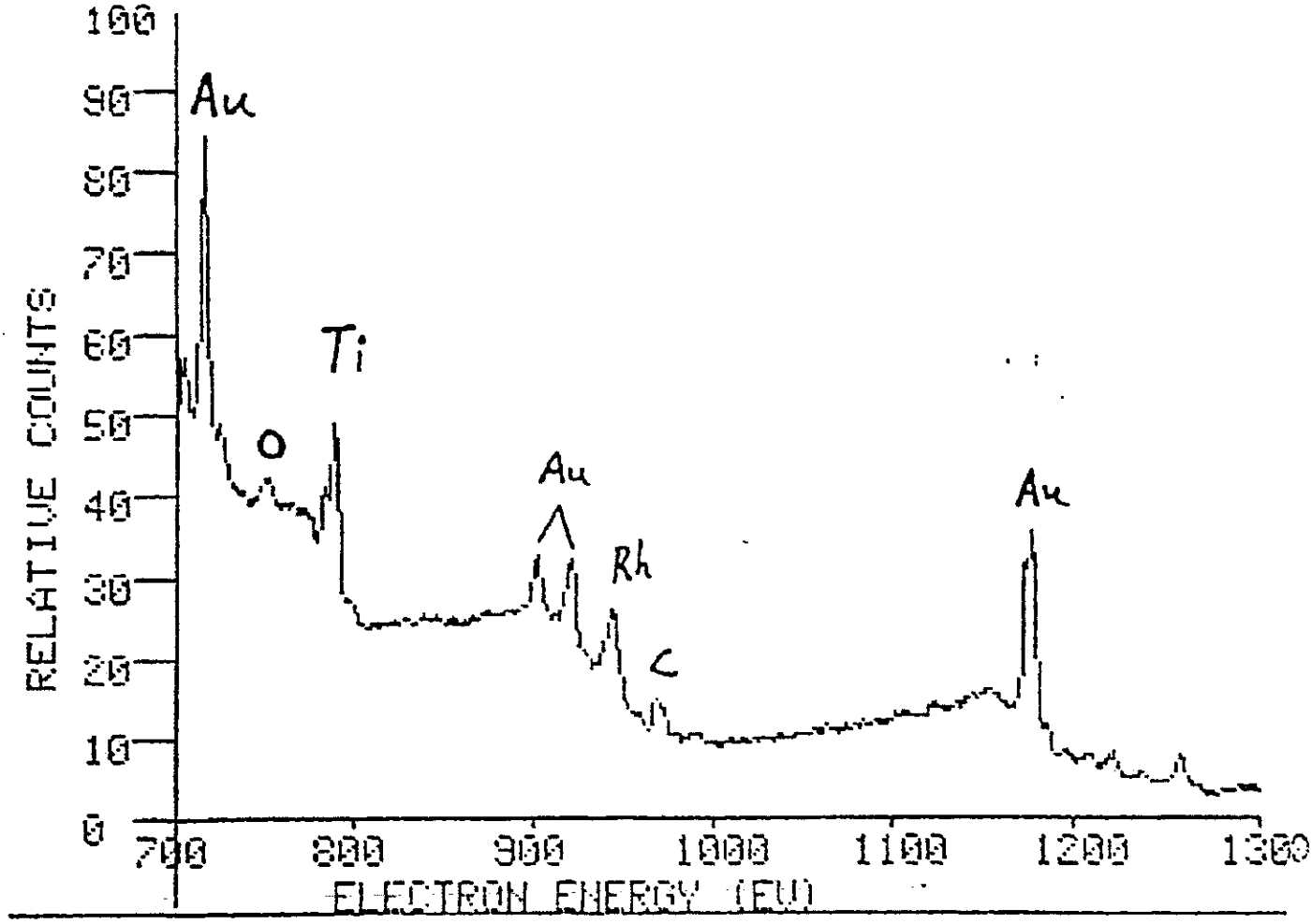

Figure 4

X-ray photoelectron spectrum of $TiRhO_3$ mounted on gold foil.

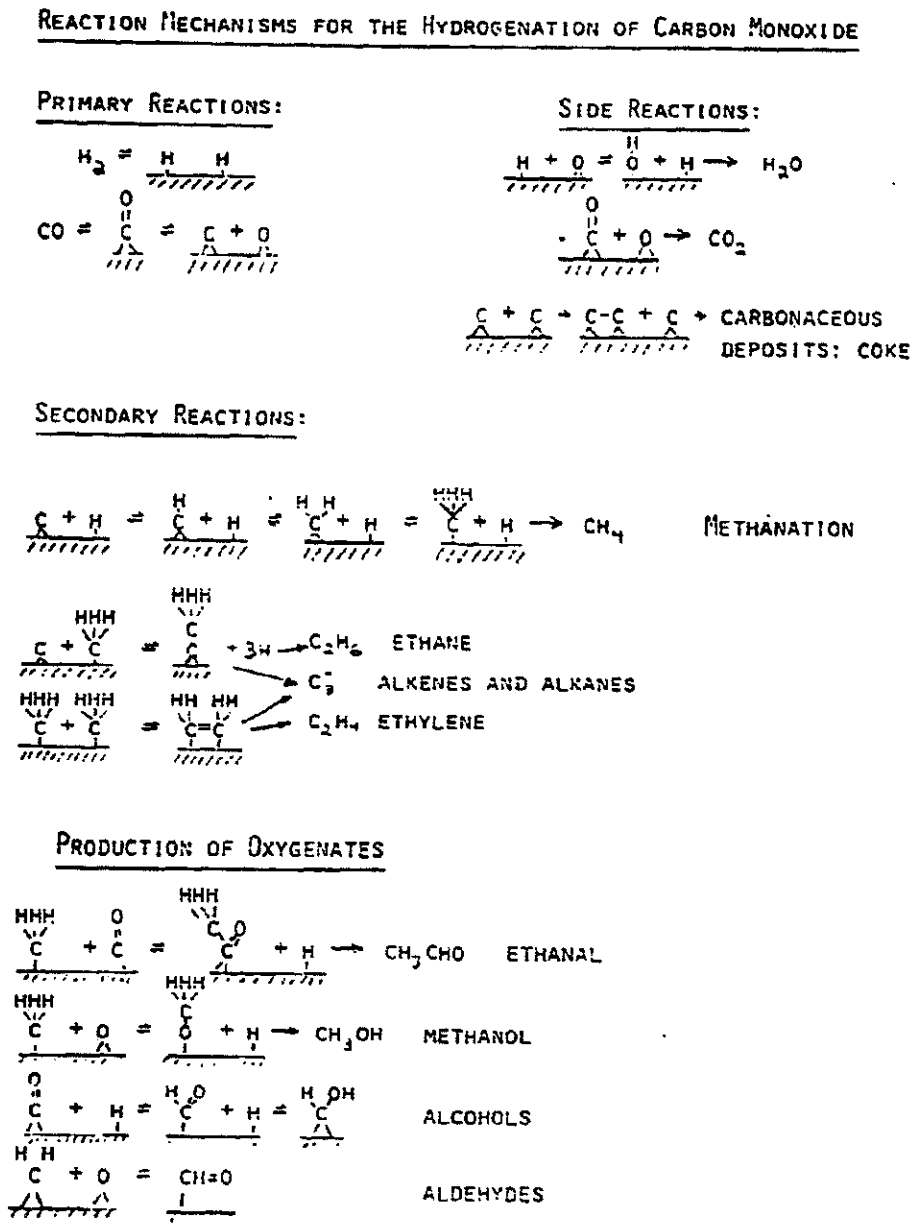

Figure 5

Possible reaction pathways for the formation of alkanes, alkenes, and oxygenated products. Also shown are the side reactions for the formation of CO_2, H_2O, and coke.

PRESSURE DEPENDENCE OF CO AND H_2 FOR METHANATION ON RHODIUM FOIL

$$R_{CH_4} = K P_{CO}^{-1} P_{H_2}^{+1}$$

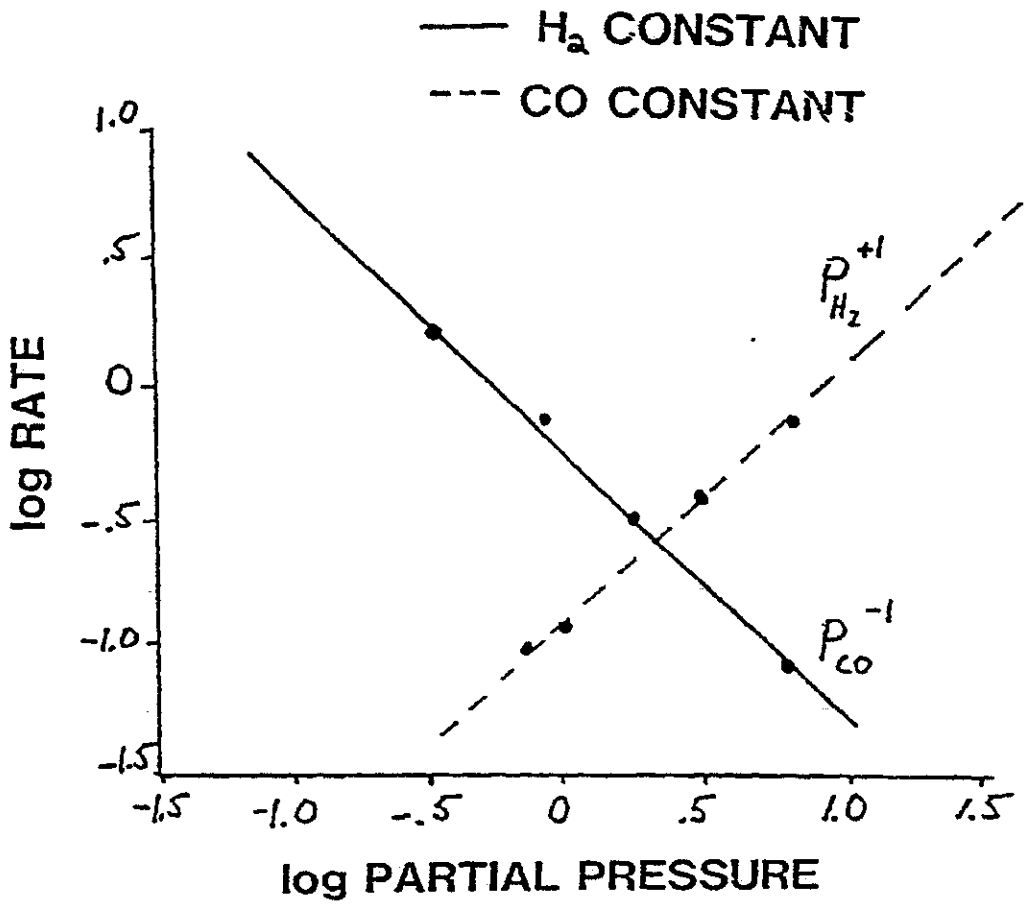

Figure 6

Experimental plot to determine the rate expression for methanation on rhodium foil.

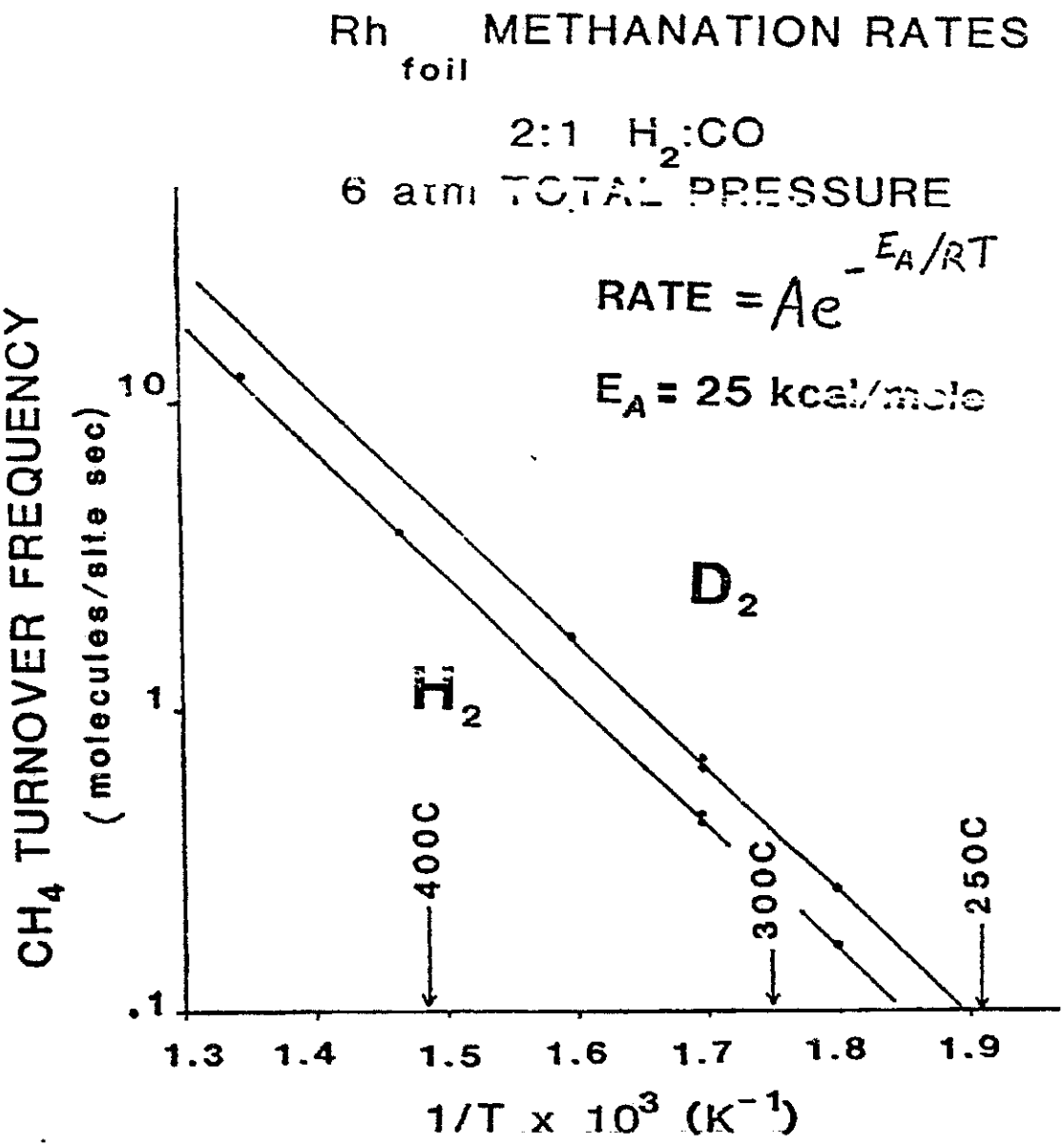

Figure 7

Rates for methanation are plotted versus temperature showing the inverse deuterium effect.

OXIDE PREPARATION / CHARACTERIZATION

1) MIX WATER SOLUBLE SALTS

2) PRECIPITATE WITH AMMONIUM CARBONATE

3) FIRE CARBONATE PRECIPITATE AT 500°C
(IN AIR FOR 12 HOURS)

4) GRIND OXIDE TO PASS THROUGH 400 MESH SCREEN

5) CHARACTERIZE OXIDE WITH
   A) SEM
   B) X-RAY DIFFRACTION

6) BET SURFACE AREA DETERMINATION

7) MOUNT ON GOLD FOIL

8) AUGER ELECTRON SPECTROSCOPY

9) X-RAY PHOTOELECTRON SPECTROSCOPY

Figure 8
Procedure for preparing and characterizing oxide samples.

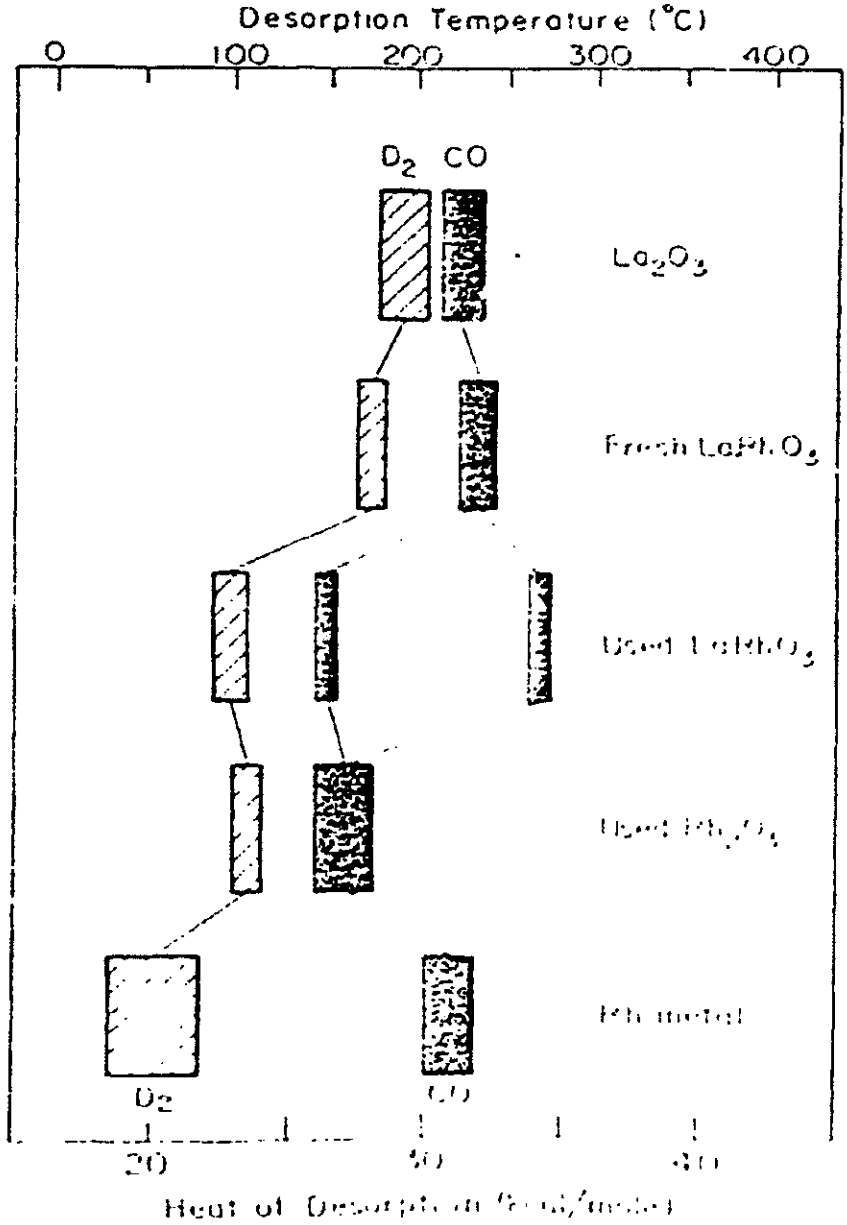

Figure 9

Thermal desorption results from CO and D_2 showing the two binding states of CO on the used $LaRhO_3$ catalyst. Also an apparent correlation between the D_2 heat of desorption and the oxidation state of rhodium on the surface can be seen.

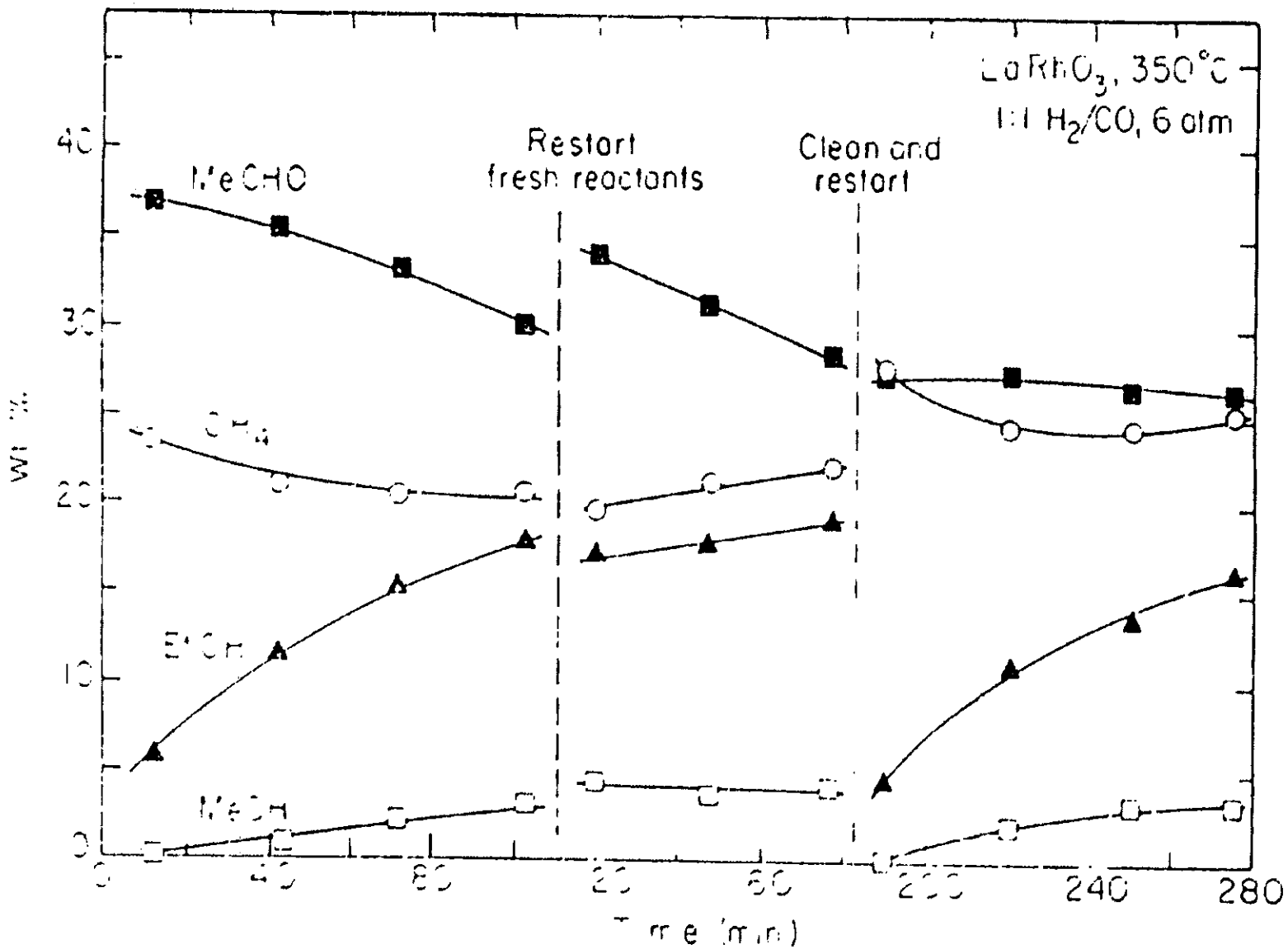

Figure 19

The change in product distribution with time is shown for methane, methanol, ethanal, and ethanol, showing the effect of replenishing the reactants, and cleaning the sample and using fresh reactants.

Compound	Rh_{foil}	Na_2RhO_3	$TiRhO_3$	$CuRh_2O_4$	$FeRhO_3$	$LaRhO_3$
CH_4 Turnover Frequency	0.37	0.08	0.07	~0.001	0.03	0.06

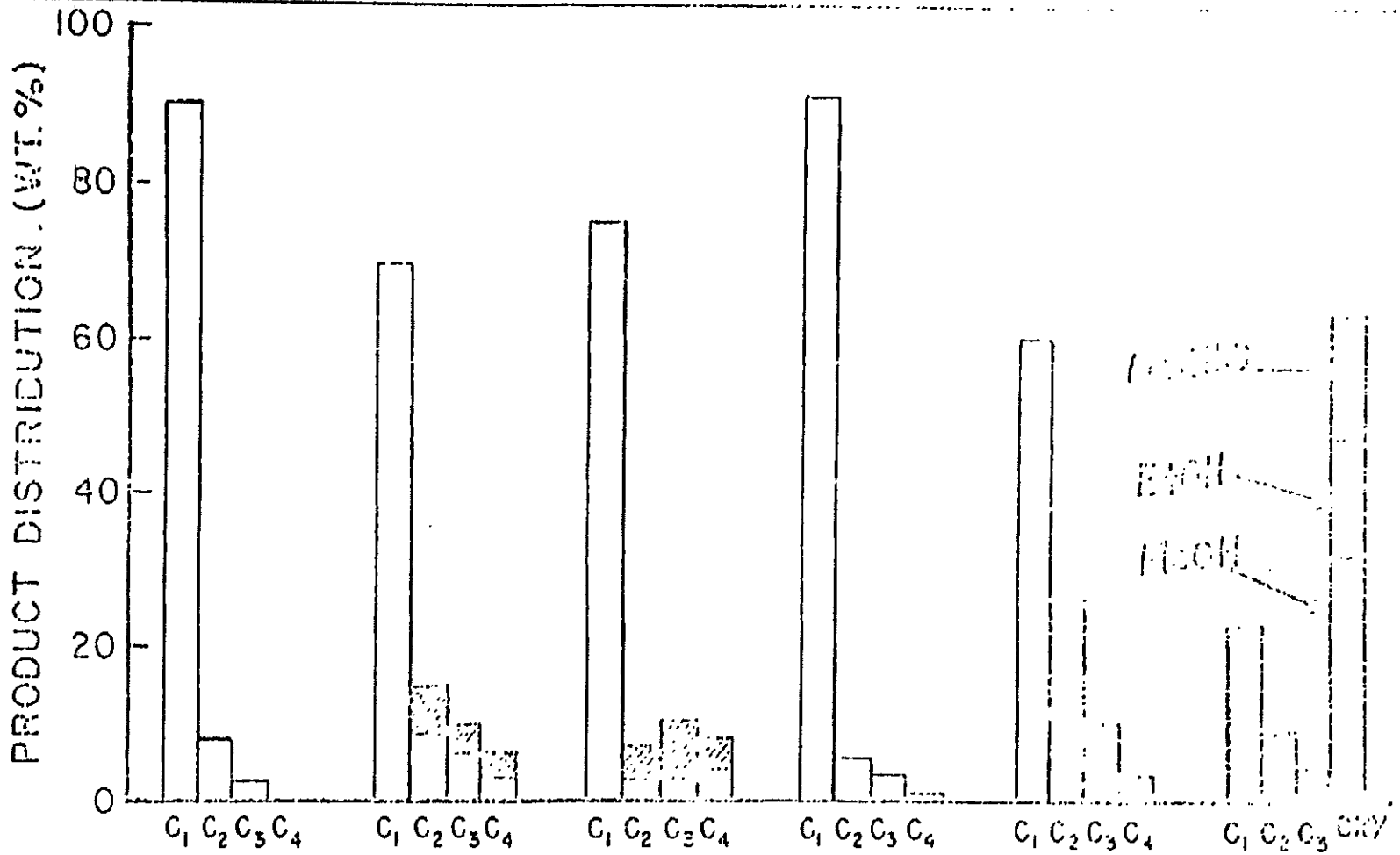

Figure 11

Product distributions for several rhodium compounds. CH_4 turnover frequency = molecules of CH_4 produced per site per second. Shaded areas represent alkene formation while open areas represent alkane formation.

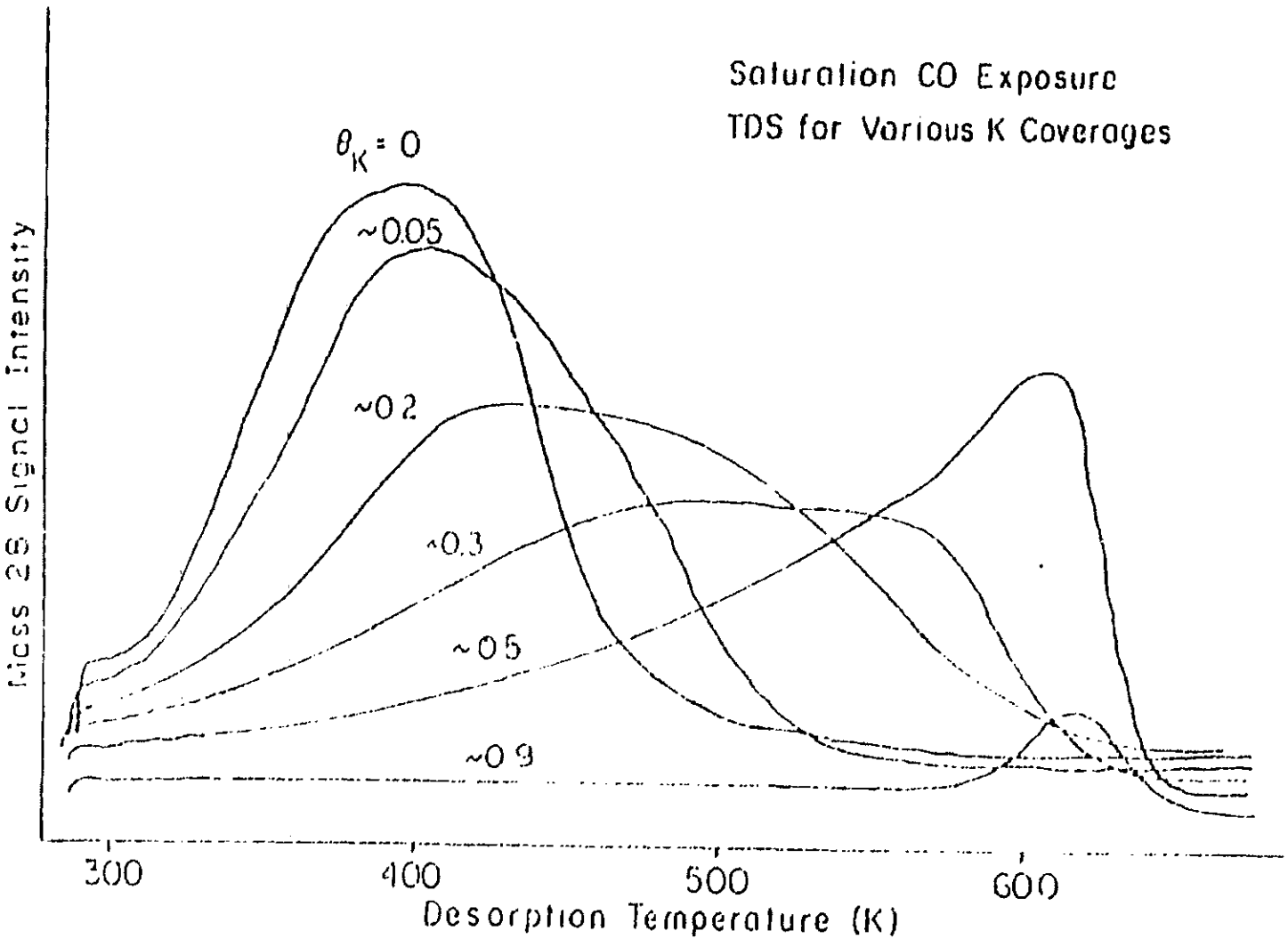

XBL 819-6461B

Figure 12

CO thermal desorption spectra with various potassium coverages, after saturation CO exposures (~10 L).

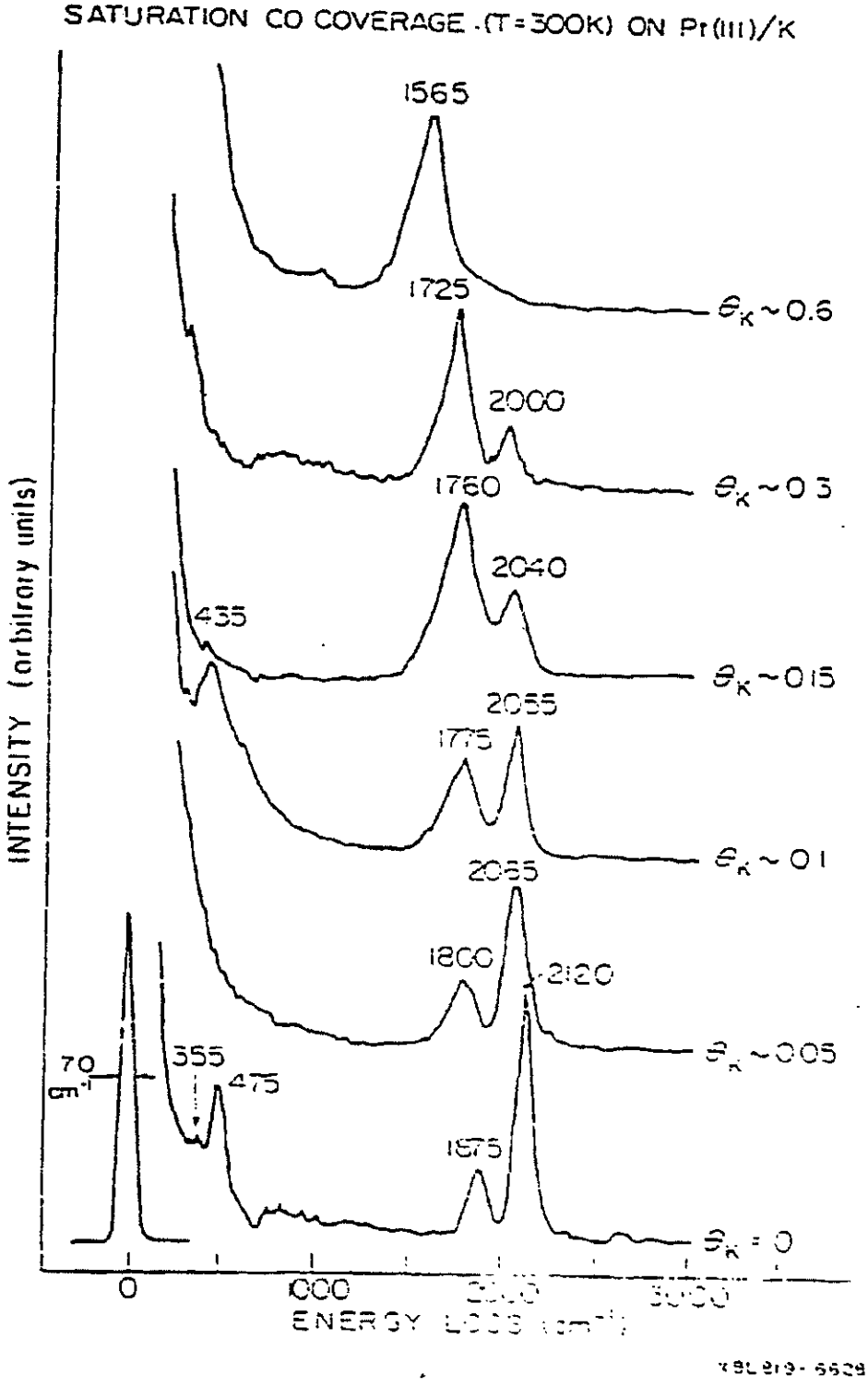

Figure 13

HREELS spectra for saturation CO exposures with various potassium coverages.

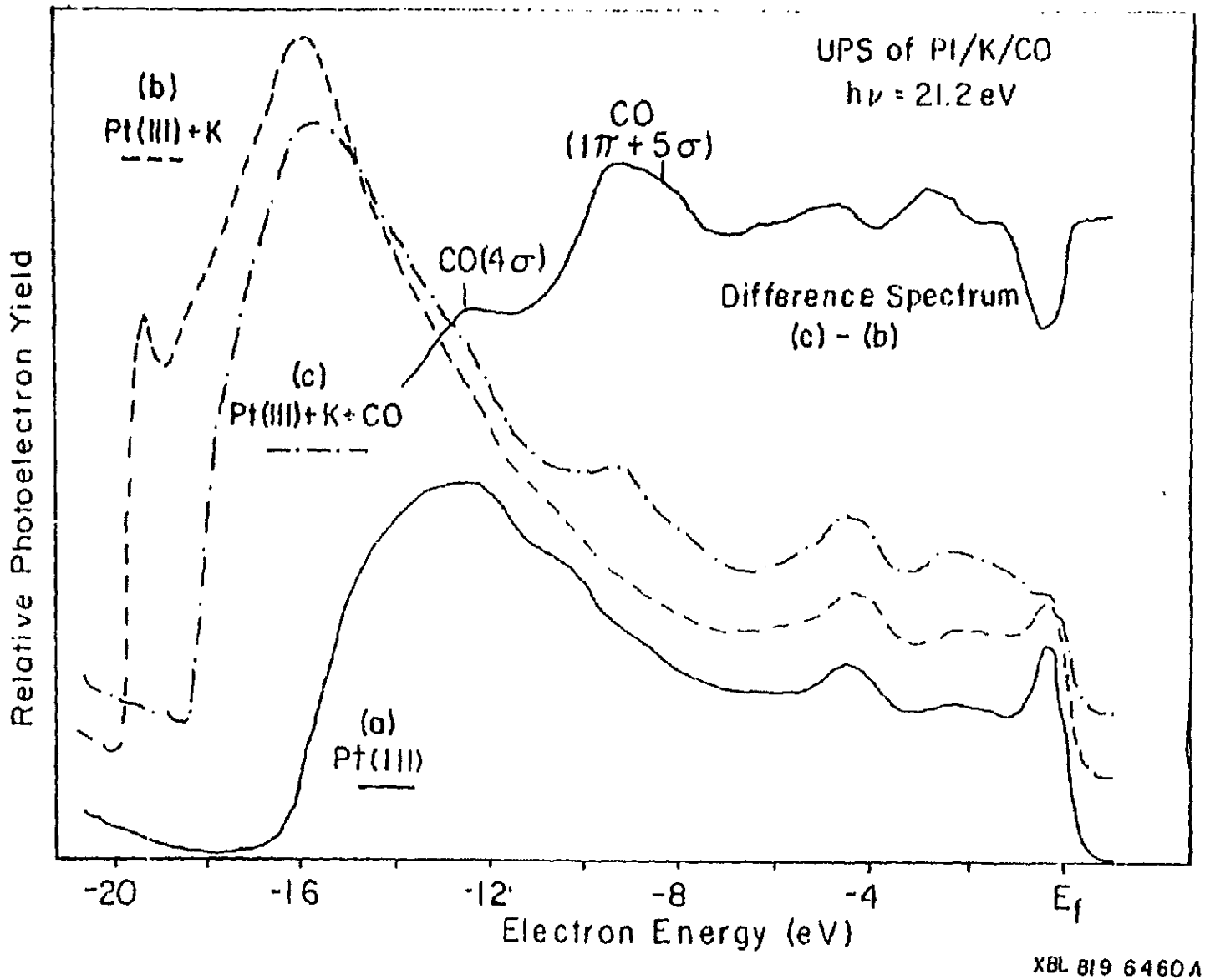

Figure 14

UPS spectra for (a) the potassium free Pt(111) surface, (b) the Pt(111) surface with θ_K=0.33, and (c) the θ_K=0.33 surface after exposure to 10L of CO. Note the change in work function.

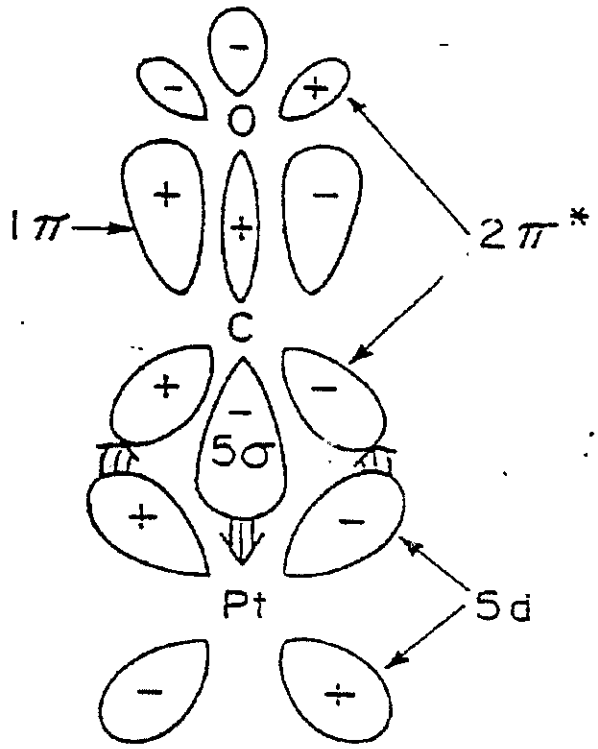

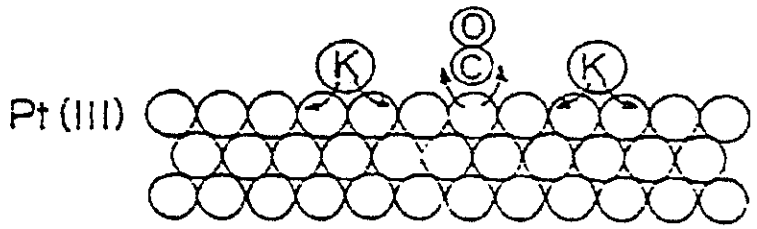

XBL823-8332

Figure 15

(a) A model of the electron orbitals believed to interact most strongly in the bonding of CO to platinum. (b) A schematic diagram of electron transfer in the Pt(111)/K/CO system.

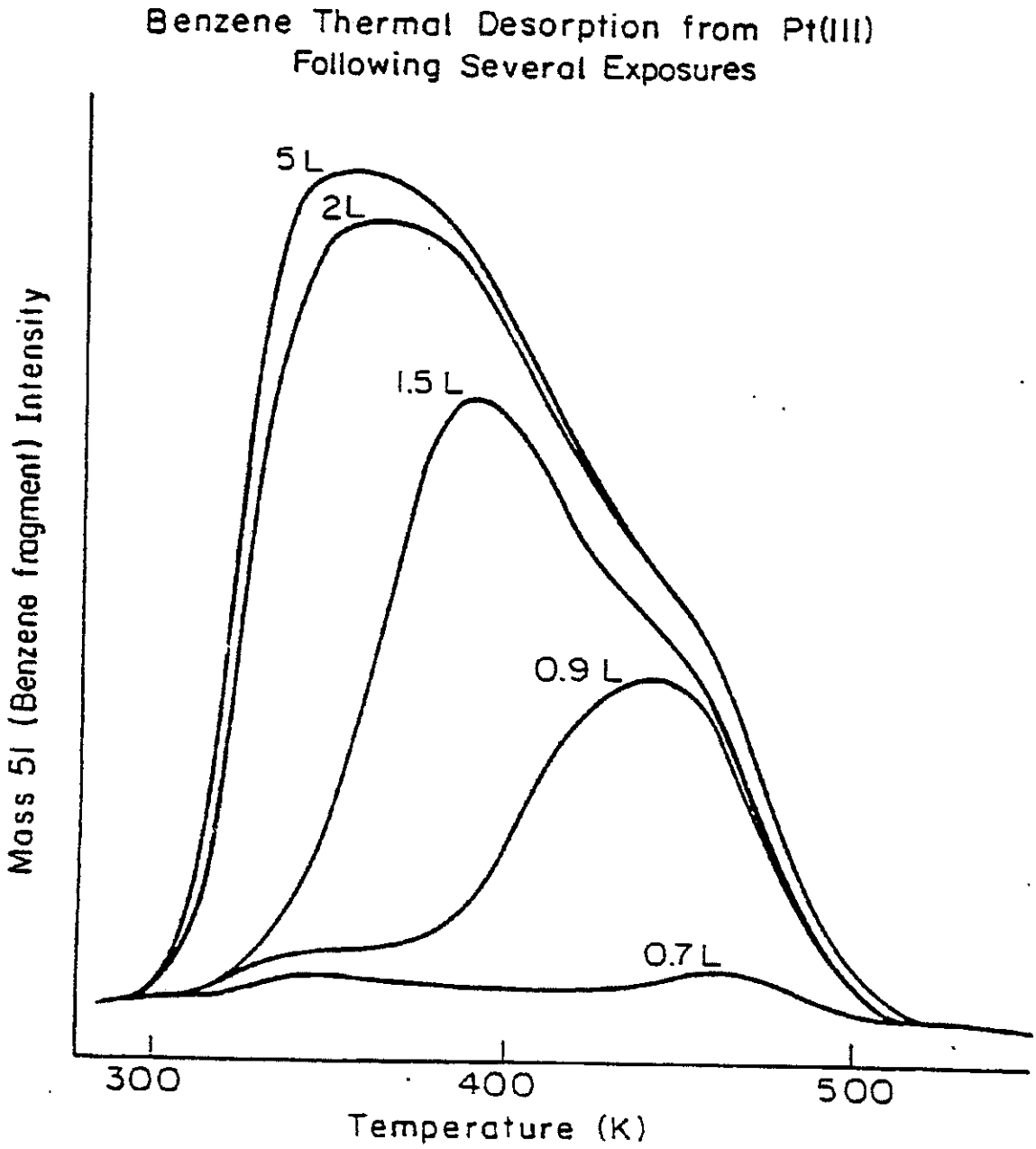

Figure 16
Benzene thermal desorption spectra following several exposures.

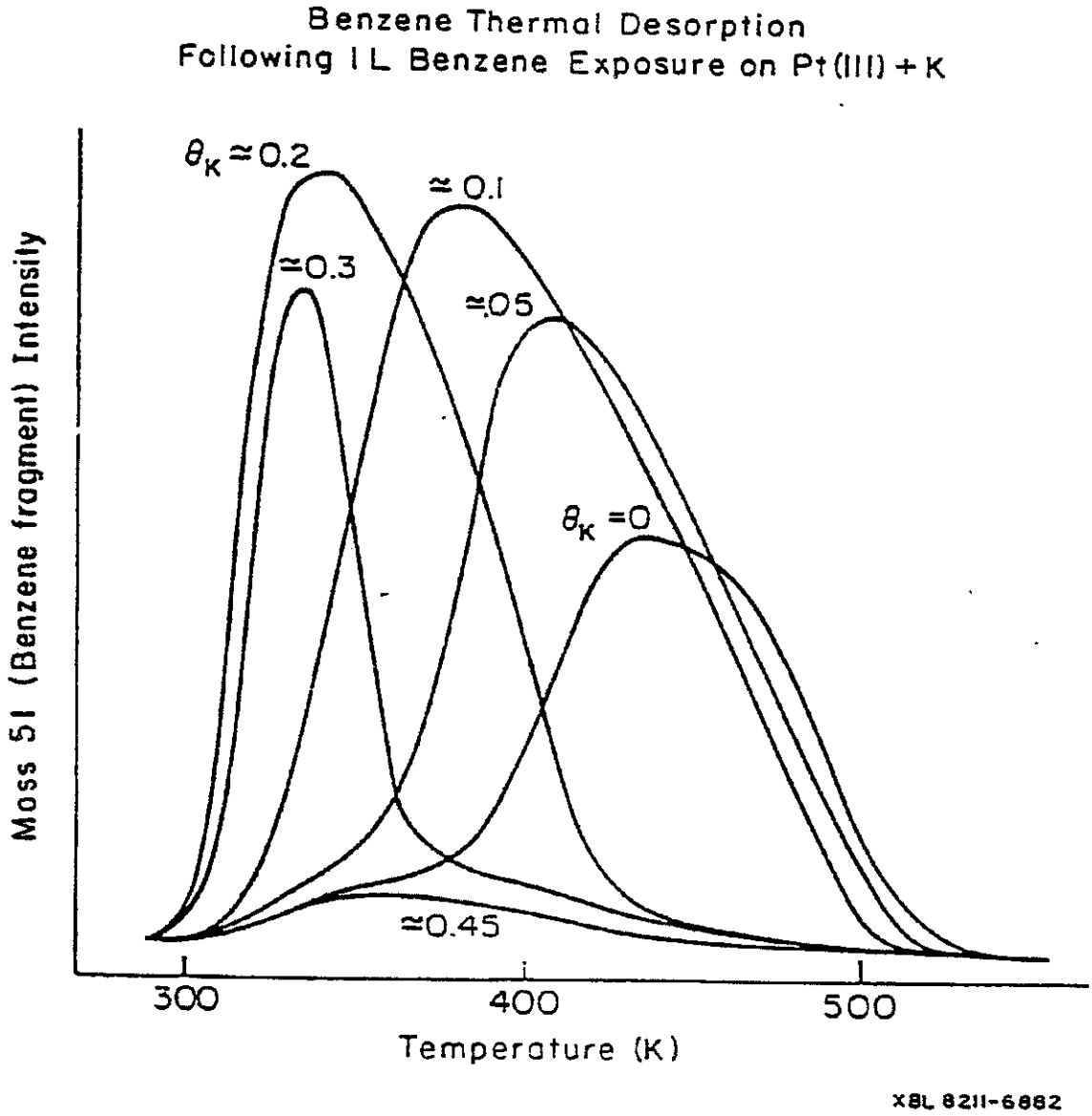

Figure 17

Benzene TDS from Pt(111) following 5 L exposures. (Heating rate = 30 K/s). Note that a potassium monolayer (saturation) is defined such that θ_K=1 and is about 1/3 the atomic density of the platinum surface layer.

Valence Orbitals of Benzene-Cr: Energy levels are approximate

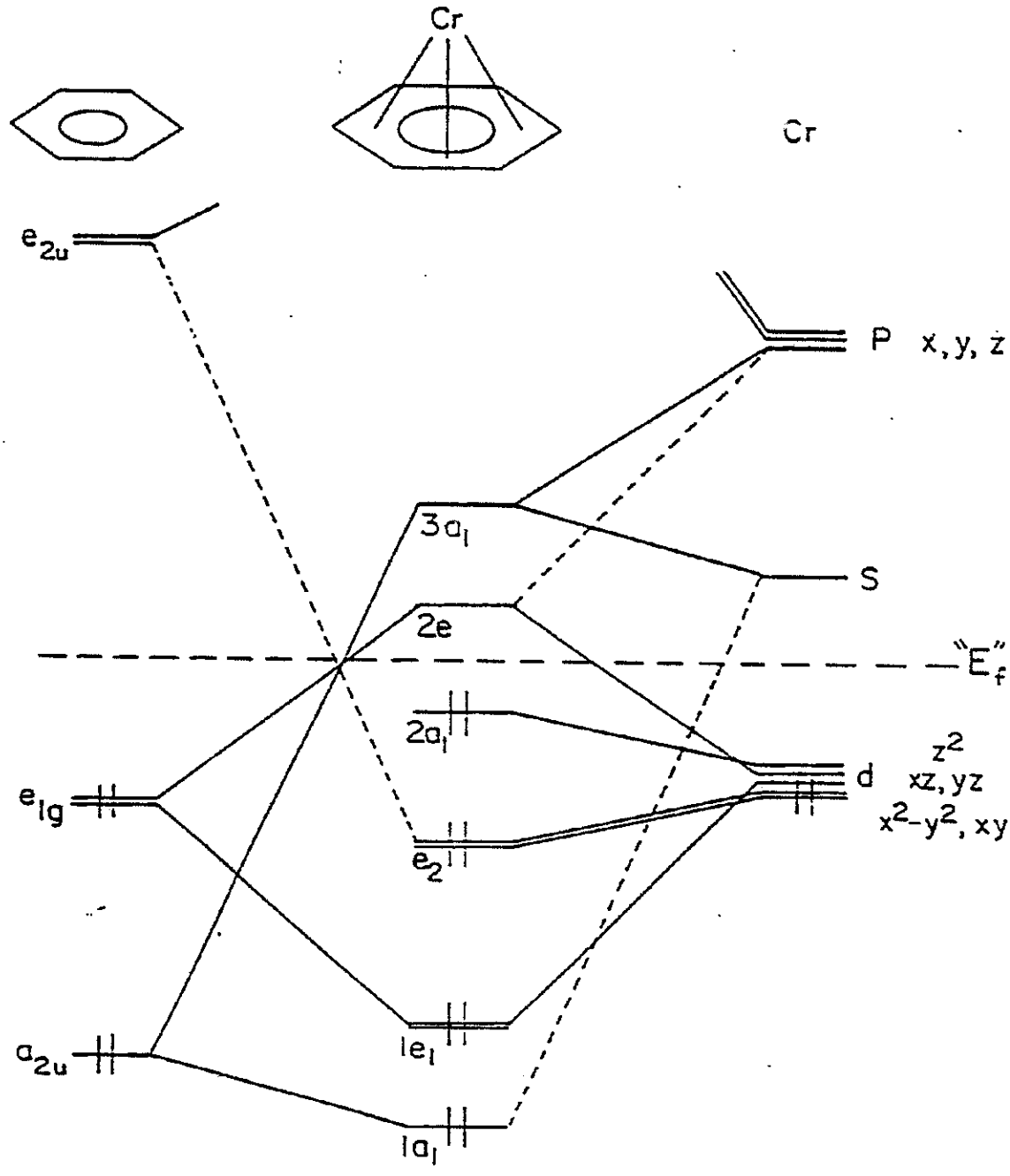

XBL 8211-6884

Figure 18

Molecular orbital correlation diagram for dibenzene-chromium

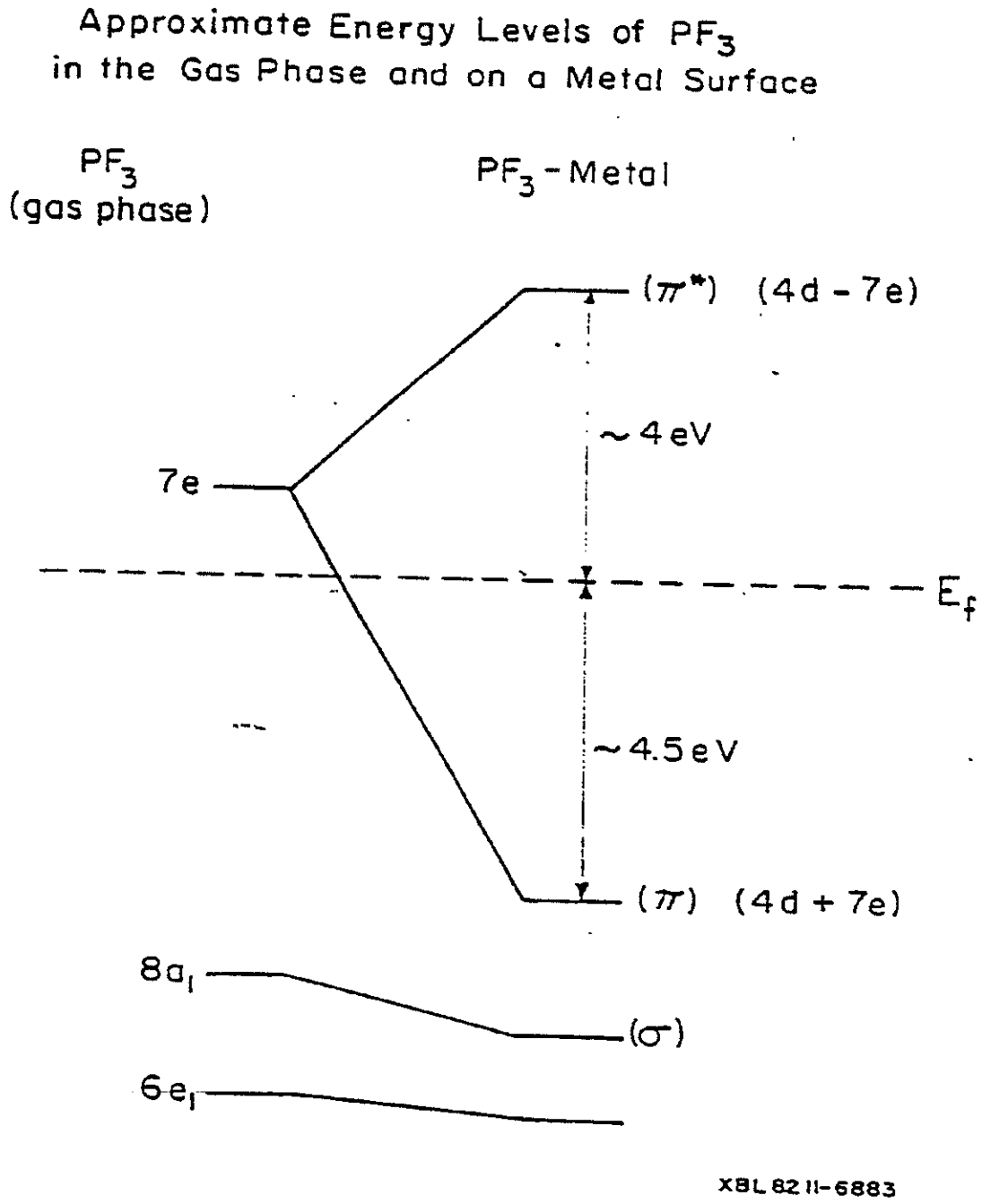

Figure 19
Approximate positions of orbital energies for PF_3. Both gas phase and chemisorption positions are given.

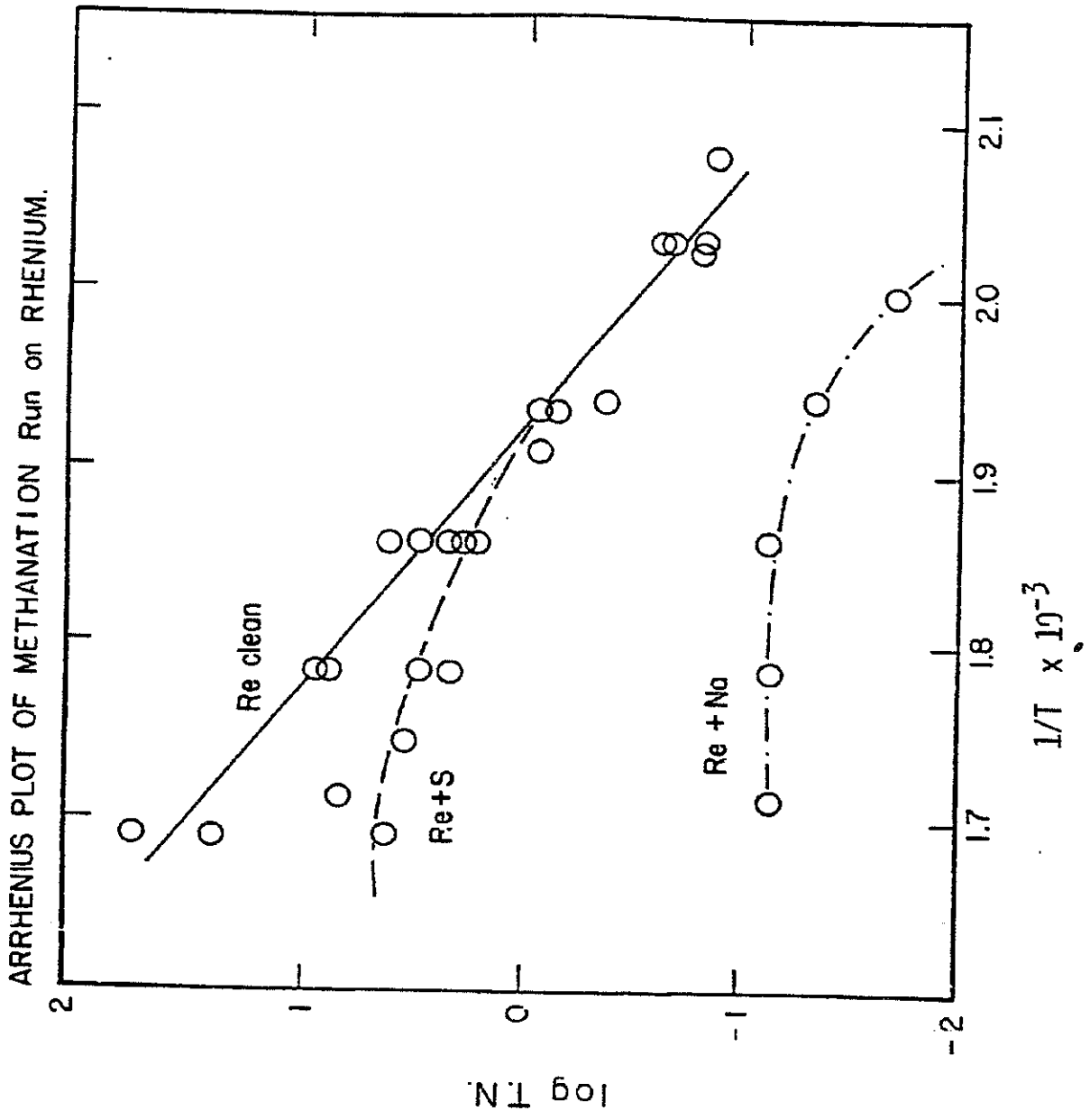

Figure 20

Arrhenius plot of the ln of the methane turnover number versus 1/T. Note the bending at high T which implies poisoning.

PRODUCT SELECTIVITIES FOR CO HYDROGENATION ON IRON AND RHENIUM FOILS WITH ALKALI OXIDE PROMOTERS. 550K; 2 ATM TOTAL PRESSURE; $CO/H_2=1/4$

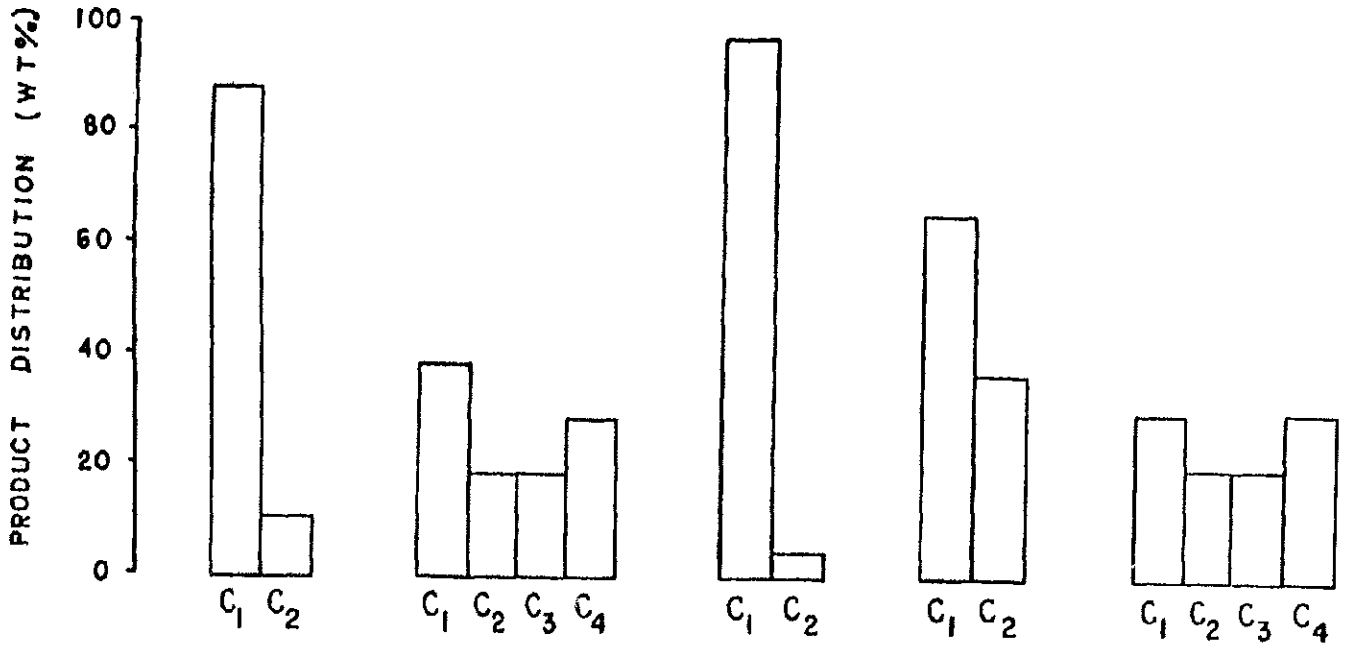

	Re foil	Fe foil	Re O_x	Re + NaO_x	Fe + KO_x
Turnover Freq. at 550K	1-2	5-6	(?surf. area)	.1	2-15 (?surf area)
Activation Energy for methanation	28 kcal/mole	24		(Poisoning)	30 (Poisoning)
C_A (ethylene)	21	17			

Figure 21

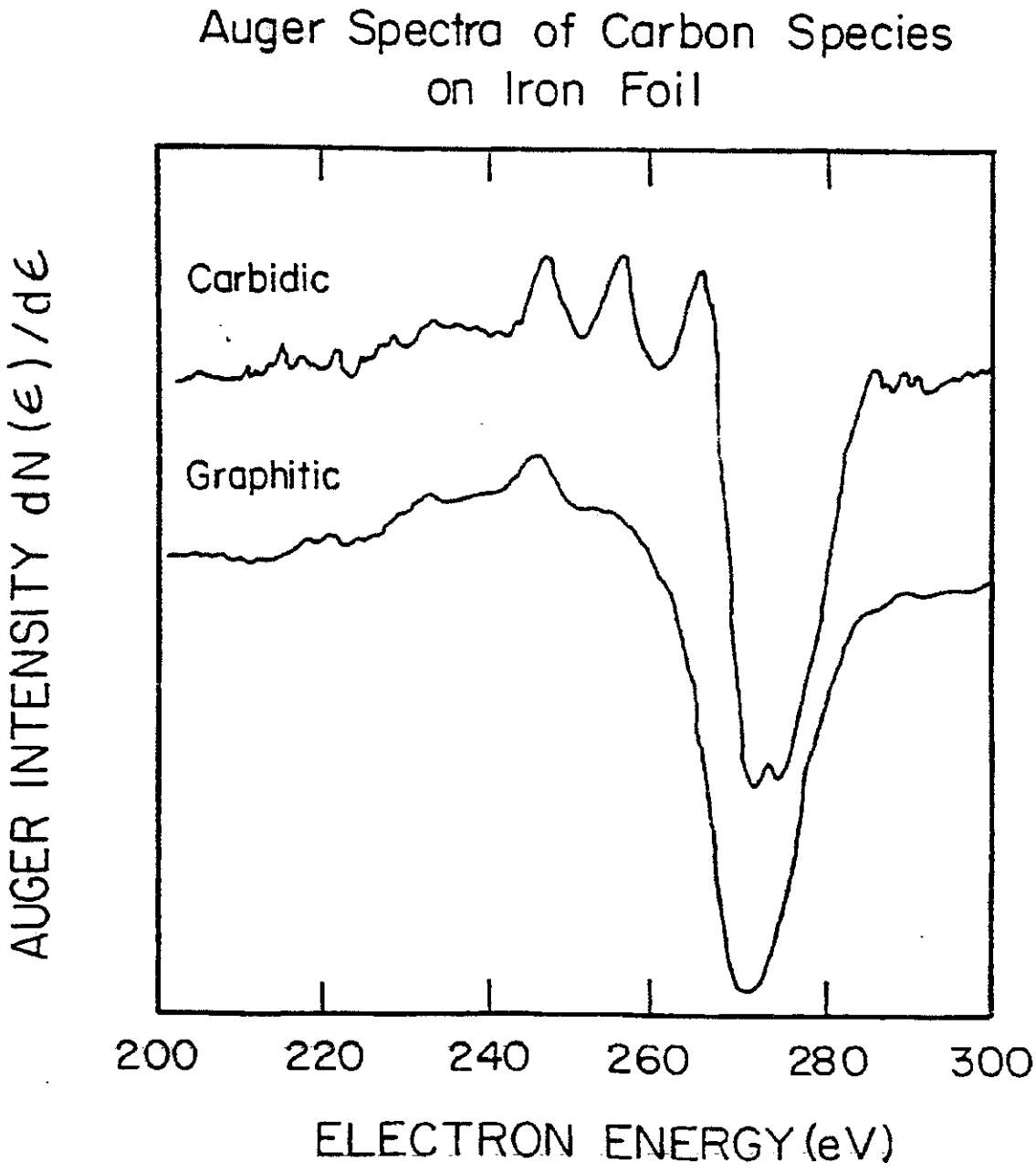

Figure 22

Sample of carbon species found on surface after reactions. Carbidic is an active carbon, while graphitic is relatively inactive to hydrogenation or oxidation.